



0017-9310(94)E0013-K

# Heat transfer of an impinging jet on a flat surface

LIANMIN HUANG and MOHAMED S. EL-GENK†

Institute for Space Nuclear Power Studies, The University of New Mexico, Albuquerque, NM 87131, U.S.A.

(Received 14 September 1993 and in final form 6 December 1993)

**Abstract**—Heat transfer between a uniformly heated flat plate and an impinging circular air jet was investigated experimentally to determine the values of the local and average Nusselt numbers, particularly for small values of Reynolds number and jet spacing. A heat transfer correlation was developed, which extends the existing database to Reynolds number and jet spacing values as low as 6000 and one jet diameter, respectively. Experimental results provided useful information of interest to potential industrial applications regarding the radius of the heat transfer area and jet spacing for maximizing the average Nusselt number.

## INTRODUCTION

BECAUSE of its importance to many industrial applications, heat transfer between a single and multiple impinging air jets and a flat surface has been the subject of numerous investigation over the past four decades [1–9]. Examples of impinging air jets applications include cooling of electronic equipment, drying of paper and textiles, and cooling of critical parts of high temperature turbines.

Gardon and Akfirtat [3] have investigated the effect of turbulence on local heat transfer coefficient of impinging jets. They concluded that the heat transfer characteristics of impinging jets cannot be explained in terms of velocity and position-dependent boundary layer alone, but by accounting for the influence of turbulence. The later appeared to be uniquely dependent on the jet Reynolds number.

Goldstein *et al.* [9] experimentally investigated the heat transfer between a single circular air jet impinging on a heated flat plate that is 0.2405 m wide and 0.107 m long. In these high Reynolds number experiments ( $6.1 \times 10^4 \leq Re \leq 1.24 \times 10^5$ ), the maximum stagnation Nusselt number (at  $R = 0$ ) occurred at  $H \approx 8$ , which is slightly higher than earlier values,  $H \approx 6$ –7 by Gardon [2] and  $H \approx 6$  by Tataoka [4].

Although extensive research has been performed demonstrating the strong dependence of  $Nu$  and  $Nu_{max}$  on both  $H$  and  $R$ , very little data have been reported of their effects on  $\bar{Nu}$  and  $\bar{Nu}_{max}$ , which could be important in some practical applications. Goldstein *et al.* [10] have shown that for  $Re \geq 61\,000$  and for  $2 \leq H \leq 5$ ,  $Nu_{max}$  always occurred at  $R \approx 2$ . However, they correlated the heat transfer data only for  $H \geq 6$  and  $0.5 \leq R \leq 32$ , indicating that  $\bar{Nu}$  values were best

correlated in terms of  $Re^{0.76}$ . Their results showed that  $\bar{Nu}$  depends on both  $H$  and  $R$ , and  $\bar{Nu}_{max}$  always occurred at  $H = 7.75$ , regardless of the value of  $R$ .

In an earlier correlation by Schlunder [5], which was based on experimental data for  $2 \leq H \leq 12$ ,  $2000 \leq Re \leq 400\,000$ , and  $2.5 \leq R \leq 7.5$ ,  $\bar{Nu}$  was expressed in terms of a complicated function of  $Re$ . Unlike the correlation of Goldstein *et al.* [10], in Schlunder's correlation  $\bar{Nu}$  decreased monotonically with both  $H$  and  $R$ . In addition to the indicated difference of the effects of  $H$  and  $R$  on  $\bar{Nu}$ , the correlations of Goldstein [10] and Schlunder [5] gave very different predictions of  $Nu$  for  $H < 6$  (see result section for details). Most recently, Jambunathan *et al.* [11] suggested that local Nusselt number was proportional to  $Re^p$ , and the exponent  $p$  was a function of  $R$  and  $H$ . This means that the dependence of Nusselt number on Reynolds number is influenced by the geometric conditions of impingement system. This result is very different from previous investigations, [5, 10]. Therefore, the effects of both  $H$  and  $R$  on  $\bar{Nu}$  and  $\bar{Nu}_{max}$ , particularly for small values of  $H$  and  $Re$ , require further investigation.

This paper presents the results of an experimental investigation of a uniformly heated flat plate impinged by a perpendicularly circular air jet at low  $H$  and  $Re$  values. In the experiments,  $R$  was varied from 0 to 10,  $H$  from 1 to 12 and  $Re$  from 6000 to 60 000. These values of  $Re$  are lower than those investigated by Goldstein *et al.* [10], but overlap with those of Schlunder [5]. In addition to correlating  $\bar{Nu}$  data for the entire range of experimental parameters, the effects of  $H$  and  $R$  on both  $\bar{Nu}$  and  $\bar{Nu}_{max}$  were investigated. The correlation was compared with those of Goldstein [10] and Schlunder [5] to determine the effects of  $R$  on  $\bar{Nu}$  at low Reynolds numbers.

† Author to whom correspondence should be addressed.

## NOMENCLATURE

$a$	coefficient in equation (3a)	$r_0$	radius of heat transfer surface [m]
$A$	heat transfer area [m <sup>2</sup> ]	$R$	dimensionless radial distance from stagnation point, $r/d$
$b$	coefficient in equation (3b)	$Re$	Reynolds number based on the diameter of the jet, $4\dot{m}/\pi d\mu$
$c$	coefficient in equation (3c)	$R_0$	dimensionless radius on heat transfer surface, $r_0/d$
$C_p$	air specific heat [J kg <sup>-1</sup> K <sup>-1</sup> ]	$T_j$	temperature of air jet [K]
$d$	jet diameter [m]	$T_w$	local temperature of heat transfer surface [K].
$h$	jet-to-plate distance [m]	Greek symbols	
$H$	dimensionless jet-to-plate spacing, $h/d$	$\rho$	air density [kg m <sup>-3</sup> ]
$H_{\max}$	dimensionless jet-to-plate spacing corresponding to $\overline{Nu}_{\max}$	$\mu$	dynamic viscosity of air [kg m <sup>-1</sup> s <sup>-1</sup> ].
$k$	air thermal conductivity [W m <sup>-1</sup> k <sup>-1</sup> ]	Subscripts	
$\dot{m}$	air mass flow rate [kg s <sup>-1</sup> ]	exp	experimental
$Nu$	local Nusselt number, $q d/k(T_w - T_j)$	cal	calculated
$\overline{Nu}$	average Nusselt number, equation (2)	max	maximum value.
$P$	electrical power to heated foil [W]		
$Pr$	Prandtl number, $\mu C_p/k$		
$q$	surface heat flux [kW m <sup>-2</sup> ]		
$Q$	volumetric flow rate of air [m <sup>3</sup> s <sup>-1</sup> ]		
$r$	radial distance from stagnation point [m]		

## EXPERIMENTAL SETUP AND PROCEDURE

The experimental apparatus, shown in Fig. 1, consisted of a heated flat plate, a jet assembly, a jet support frame, flow meters, and a data acquisition system. The air jet was formed using a Plexiglas tube, 6.2 mm in diameter and 160 mm long. This length of the jet tube was selected to ensure that the tube ratio, length-to-distance (= 25.8), is larger than that needed for

the air flow at the exit of the jet tube to reach fully developed status [12]. The jet support frame was used to adjust the elevation of the jet from the heated surface,  $H$ , and to maintain the jet in the vertical position. The heated plate was made of a 0.0508 mm thick, 321A stainless-steel foil measuring 140 × 140 mm. The foil was laid perfectly flat on a 25.4 mm thick Bakelite slab, overlaid on top of a 25.4 mm thick Plexiglas plate for thermal insulation.

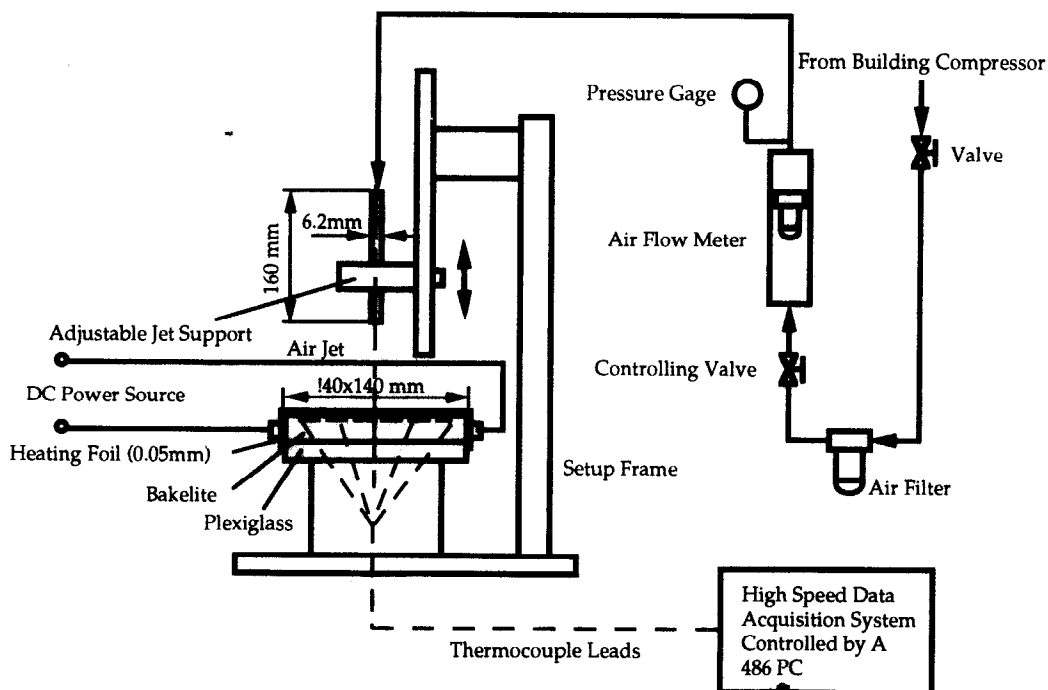


FIG. 1. A schematic of experimental setup.

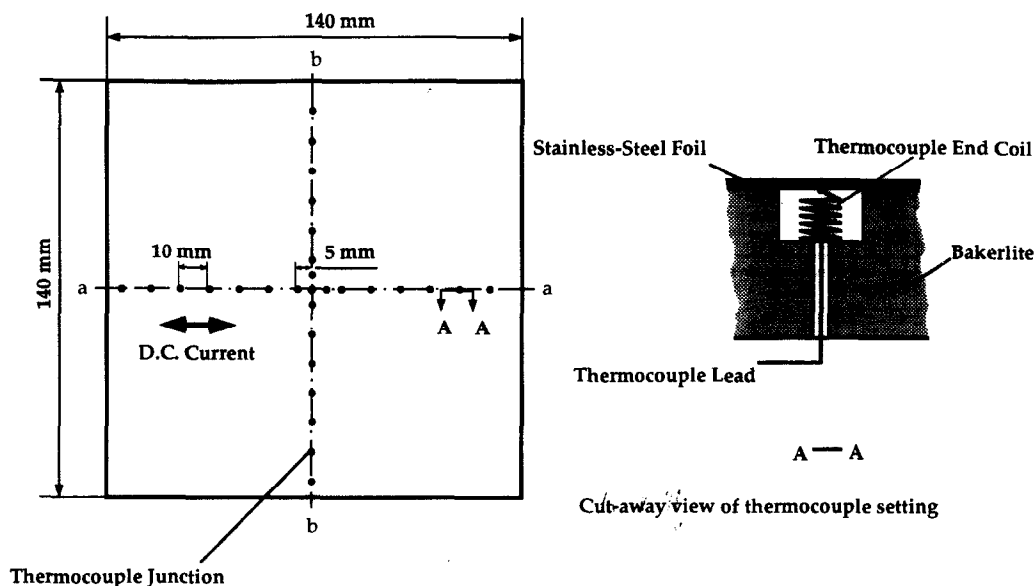


FIG. 2. Instrumented test section and thermocouple arrangement.

steel foil was heated using a high current/low voltage D.C. power supply. To examine the uniformity of surface heating and the symmetry of surface temperature, the foil temperatures were measured in two perpendicular directions using a total of 29 type-K thermocouples. The thermocouples were inserted through the upper surface of the Bakelite slab, parallel and perpendicular to the direction of the electric current (see Fig. 2). In addition to the thermocouple placed at the centre of the test section to measure the foil temperature at the stagnation point, there were a total of 14 thermocouples in each direction, spaced as shown in Fig. 2. Because the stainless-steel foil expands when heated, the ends of the thermocouple wires were made into elastic coils to provide a spring action and maintain a good contact with the underside of the heated foil during the experiments. Repetitively, experiments were performed with current flow in different directions to assess the influence of any induced voltage on the thermocouple readings. No notable changes in the values of the measured temperatures were detected.

In the experiments, the air from the building compressor was filtered to remove moisture before entering the flowmeters. Air rotameters were used to measure the air volumetric flow rate, which was corrected using the measured air temperature and pressure after exiting the flowmeters (see Fig. 1). A high speed data acquisition system controlled by a 486 PC was used to monitor all thermocouples and collect experimental data. During the experiments, the measured temperature distributions in the heated plate were displayed at real time on the computer monitor to ensure proper setup of the experiments and stability of measurements. Although the ambient temperature was not controlled in the experiments, the difference between the air temperatures at the jet exit and the

ambient was less than  $\pm 1.0$  K; hence, the effect of entrainment on the heat transfer coefficient would be insignificant.

The controlled parameters in the experiments were the jet spacing, electric power input, and the air volumetric flow rate. In all experiments, the centerline of the jet was lined up with the center of the heated surface. At each power level, the air flow rate was adjusted and kept constant. After reaching steady-state, the electric power input, air flow rate, foil surface temperatures, and air temperatures at jet exit were recorded. The input power was increased in small increments from 50 to 220 W, which corresponds to surface heat flux of 2.3–10.2 kW m<sup>-2</sup>. The heat loss due to radiation was negligible and that due to thermal conduction through the Bakelite and Plexiglas was less than 2%. Based on pre-experiment calibration, the uncertainties were about  $\pm 0.4^\circ\text{C}$  in temperature measurements,  $\pm 4.5\%$  in air volumetric flow rates, and  $\pm 0.7\%$  in electric power. Using the methodology outlined by Holman [13] and conducting repeatable experiments, the uncertainties in  $Nu$  and  $Re$  were  $\pm 4\%$  and  $\pm 5\%$ , respectively.

## RESULTS AND DISCUSSION

A total of 140 experiments were performed yielding 1200 data points. Figure 3 shows the measured radial distributions of the measured surface temperatures in the direction of the electric current (a-a) and in the perpendicular direction (b-b), at different  $H$  and  $Re$  (see Fig. 2). As shown, the surface temperature distributions were symmetric in both directions; the values were almost identical at the same radial distance from the stagnation point. These results confirmed the uniformity of the surface heat flux in experiments. Figure 3 also shows that, for  $H \geq 2.0$ , the

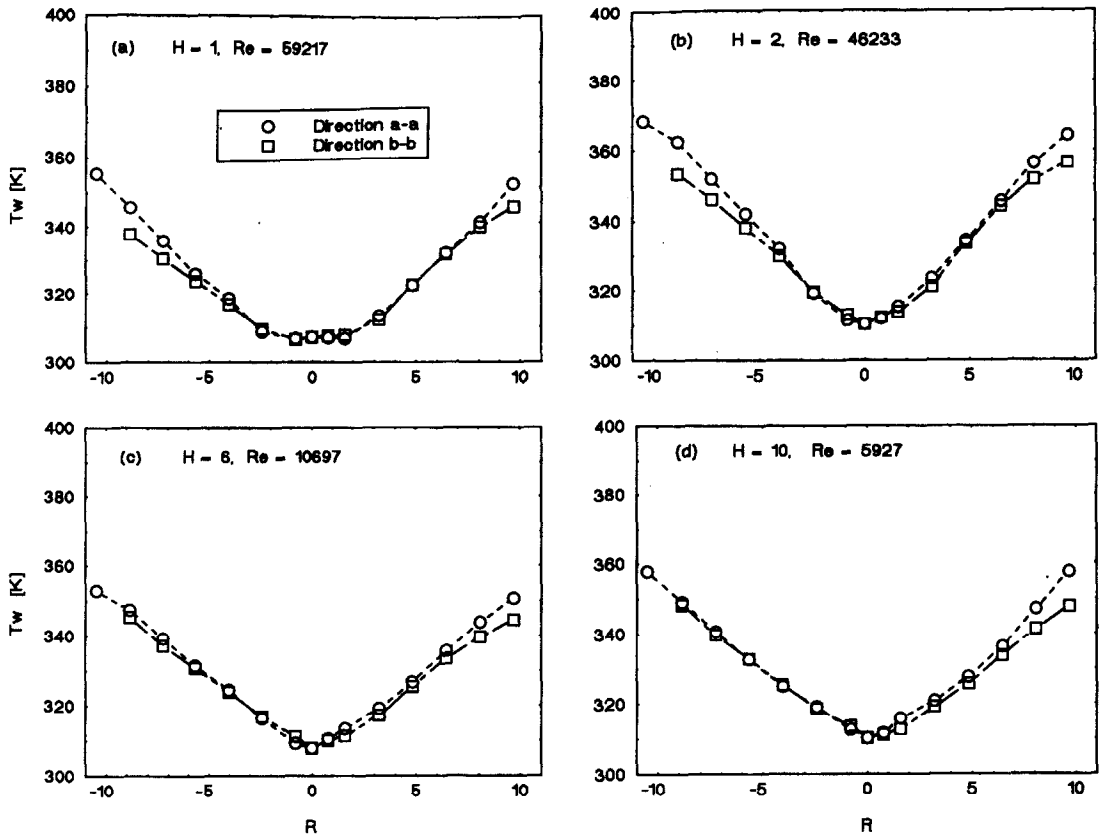


FIG. 3. Measured radial temperature distributions in the heated foil at different  $R$ .

lowest surface temperature always occurred at the stagnation point  $R = 0$ . However, for  $H = 1.0$ , the lowest surface temperature, and in turn  $Nu$ , occurred at  $R = 1.8-2$  (see Fig. 4a). The thermophysical properties of air in  $Nu$ , and  $Pr$  were evaluated at the average local film temperature,  $(T_w + T_j)/2$ , and those in  $Re$  were evaluated at the air jet temperature,  $T_j$ . Some of previous investigators defined Nusselt number in terms of the adiabatic temperature to account for compressibility effect [10]. However, in practical applications, the adiabatic temperature is not known *a priori*.

Figure 4 shows the radial distribution of  $Nu$  for different values of  $H$ . As the data in Fig. 4 indicate,  $Nu$  depends not only on  $Re$ , but also on  $H$  and  $R$ . In general,  $Nu$  increased with  $Re$ , but decreased quickly with  $R$  in the region near the stagnation point ( $R < 6$ ). For all Reynolds numbers and  $H \geq 2$ ,  $Nu_{max}$  always occurred at the stagnation point. At the smallest jet spacing ( $H = 1$ ),  $Nu_{max}$  still occurred at the stagnation point at low  $Re$  values ( $Re \leq 1.3 \times 10^4$ ); however, it shifted outward to  $R = 1.8-2.0$  as  $Re$  increased.

**CORRELATION OF AVERAGE NUSSELT NUMBER**

The experimental values of  $Nu$  were used to calculate the average Nusselt number, based on the local

temperature difference, as a function of radial distance using numerical integration as:

$$\overline{Nu}(R) = \frac{2}{R^2} \int_0^R R Nu(R) dR. \tag{1}$$

In the experiments, the local surface temperature ranged from 305 to 393 K. Similar to Goldstein *et al.* [10], the calculated values of  $Nu$  were found to be best correlated in terms of  $Re^{0.76}$  and  $Pr^{0.42}$ . However,  $\overline{Nu}$  and  $Nu_{max}$  were strong functions of both  $H$  and  $R$ . The present correlation for  $\overline{Nu}$  is as follows:

$$\overline{Nu} = Re^{0.76} Pr^{0.42} [a + bH + cH^2], \tag{2}$$

where the coefficients  $a$ ,  $b$ , and  $c$  are polynomial functions of  $R$  as:

$$a = 10^{-4} [506 + 13.3R - 19.6R^2 + 2.41R^3 - 9.04 \times 10^{-2}R^4], \tag{3a}$$

$$b = 10^{-4} [32 - 24.3R + 6.53R^2 - 0.694R^3 + 2.57 \times 10^{-2}R^4], \tag{3b}$$

and,

$$c = -3.85 \times 10^{-4} [1.147 + R]^{-0.0904}. \tag{3c}$$

These coefficients as well as the Reynolds and Prandtl number exponents in equation (2) were determined based on the best fit of the experimental data

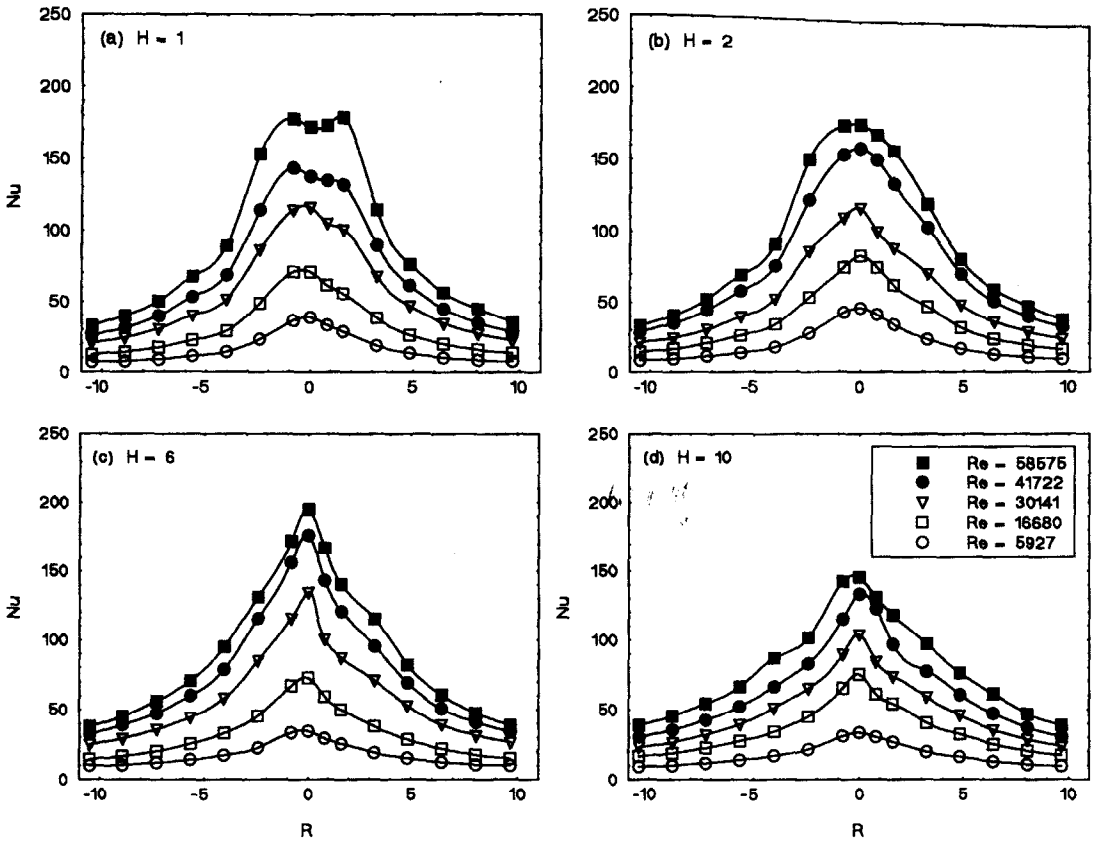


FIG. 4. Measured radial Nusselt number distributions at different  $Re$  and  $H$ .

using the least square method. It is worth noting that the exponent of Reynolds number is the same as that reported by Goldstein *et al.* [10]. As shown in Fig. 5, the agreement of correlation was within  $\pm 12\%$  of the experimental data covering the complete range of experimental parameters, except that for  $R = 0$  the agreement was within  $\pm 15\%$ . For the integral average heat transfer coefficients, the discrepancy in the stagnation

point region is of minor importance. Equation (2) extends the available heat transfer data base to  $Re$  and  $H$  as low as 6000 and 1, respectively.

**MAXIMUM AVERAGE NUSSELT NUMBER CORRELATION**

As indicated in Figs. 6 and 7,  $H$  and  $R$  significantly affected both  $Nu$  and  $\overline{Nu}_{max}$  and the maximum stag-

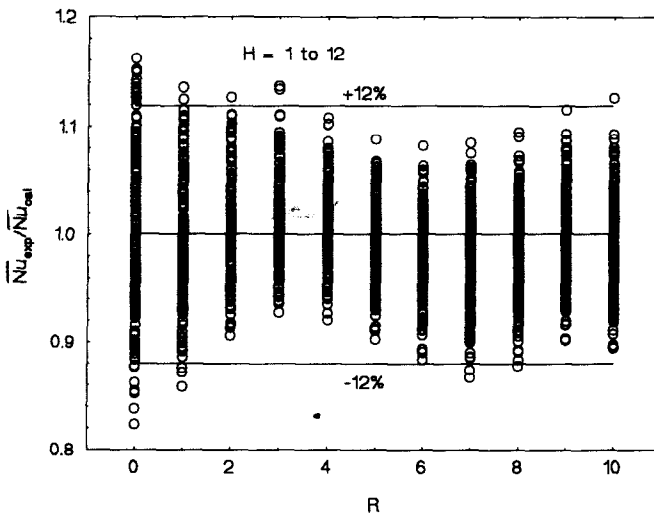


FIG. 5. Comparison of experimental data with present correlation, equation (2).

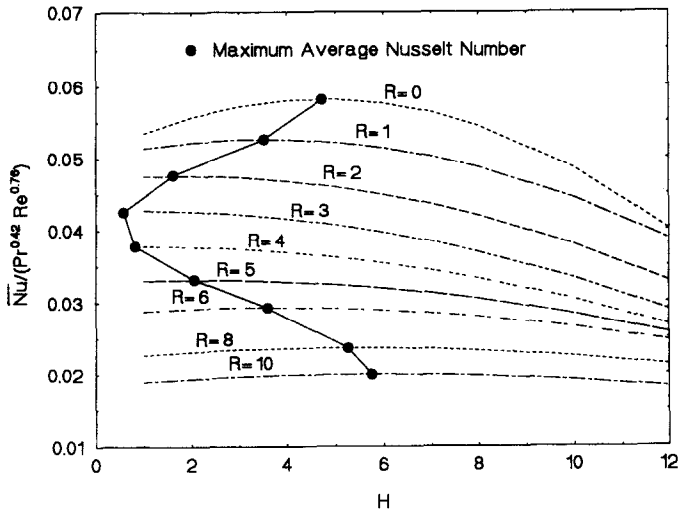


FIG. 6. Dependence of  $\overline{Nu}_{max}$  on  $H$  and  $R$ .

nation  $Nu$  occurred at  $H = 4.7$ . For given  $Re$  and  $R$ ,  $\overline{Nu}$  increased with  $H$  until it reached a maximum value, then it decreased as  $H$  was increased. The values of  $\overline{Nu}_{max}$  and the corresponding  $H_{max}$  are strong functions of  $R$ . Figure 6 shows that  $\overline{Nu}_{max}$  decreased as  $R$  was increased. However, Fig. 7 shows that  $H_{max}$  decreases from 4.7 at  $R = 0$ , to as low as 0.5 at  $R = 3.2$ , then it increased to 5.7 at  $R = 10$ . For  $H > 0.5$ , there were two values of  $R$  at which the average Nusselt number reached a maximum value. For example, at  $H = 2$ , Nusselt number reached a maximum value at  $R = 1.8$  and at  $R = 5$ ; however, the value of  $\overline{Nu}_{max}$  was higher at the former than at the latter (see Fig. 6). An expression for  $H_{max}$  as a function of  $R$  was obtained by differentiating equation (2), yielding:

$$H_{max} = -b/2c. \tag{4}$$

Equation (4) accurately predicts the values of  $H_{max}$  for the present range of  $R$  ( $0 < R < 10$ ). Equation (4),

plotted in Fig. 7, indicates the optimal combinations of  $H$  and  $R$  values corresponding to  $\overline{Nu}_{max}$ . It is worth noting that although  $H_{max}$  is independent of  $Re$  and solely dependent on  $R$ , the values of  $\overline{Nu}_{max}$  are dependent on both  $R$  and  $Re$ ; they decreased as  $R$  increased, but increased proportionally with  $Re^{0.76}$  as:

$$\overline{Nu}_{max} = Re^{0.76} Pr^{0.42} \left[ a - \frac{b^2}{4c} \right]. \tag{5}$$

The dependence of Nusselt number on  $R$  and  $H$  was caused by the flow characteristics of the impinging jet near the surface. The jet spacing has significant effect on the impinging jet flow. Schlunder [5] investigated the effect of  $H$  on the local mass (heat transfer) coefficients. He reported that at large  $H$ , say  $H > 10$ , the maximum local Sherwood number always occurred at stagnation point. However, at a small  $H$  and large  $Re$ , the maximum local Sherwood number occurred at  $R \approx 1.5-2.0$ , depending on the  $H$ . In

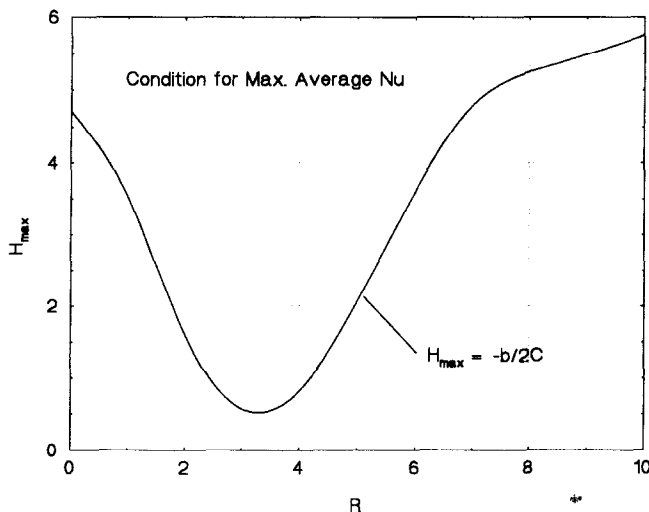


FIG. 7. Combination of  $H$  and  $R$  for  $\overline{Nu}_{max}$ .

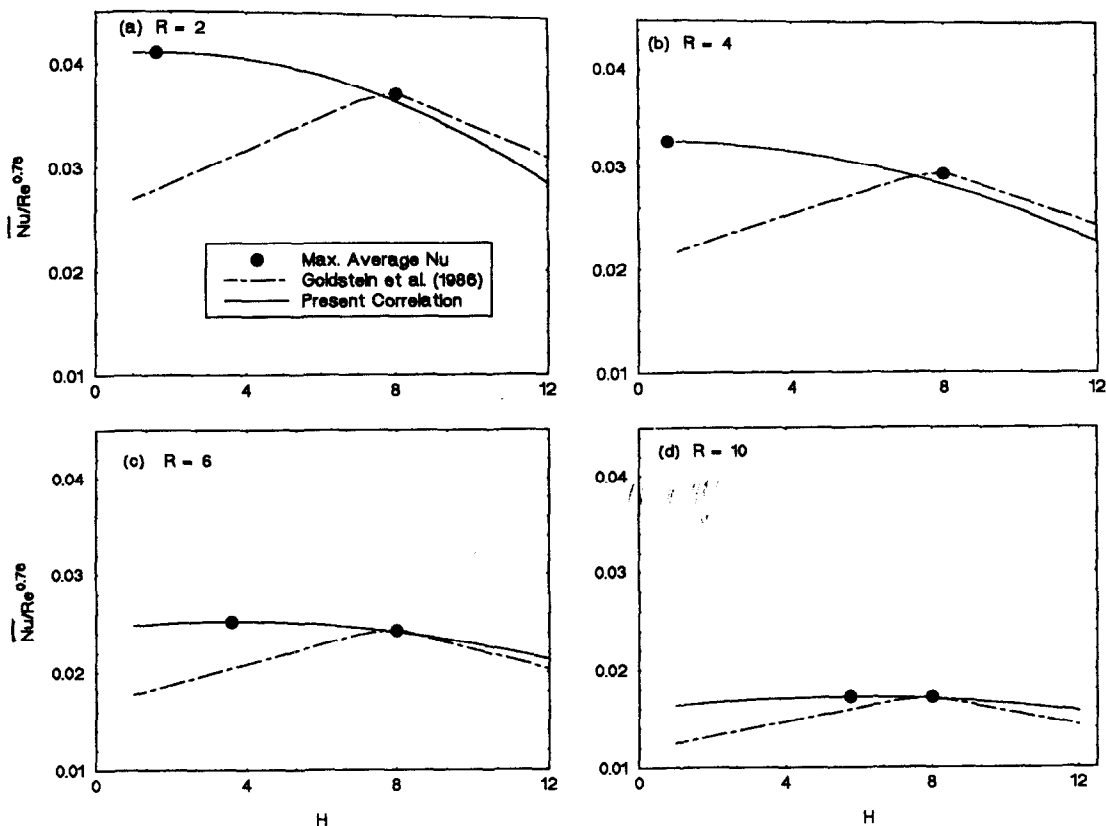


FIG. 8. Comparison of present correlation with those of Goldstein *et al.* [10].

general, the flow near the stagnation point is turbulent, resulting in a large local heat transfer coefficient. For small  $H$ , there is a certain region within which the flow parallel to the surface is accelerated. At the end of the accelerated flow region, the disappearance of the stabilizing streamwise pressure gradient leads to a sudden steep rise in the turbulence level, causing a sharp increase in the heat transfer coefficient, which may be even higher than that at the stagnation point. The accelerated flow region is influenced by the spacing  $H$ , and, therefore, the position where the maximum local Nusselt number occurs is dependent on the jet spacing,  $H$ . Since the position of  $Nu_{\max}$  moves farther from the stagnation point as spacing  $H$  is decreased, the  $H_{\max}$  corresponding to the  $Nu_{\max}$  decreases with  $R$  when  $R < 3.2$ . This behavior dominates the relationship between the  $Nu_{\max}$  and  $H_{\max}$  for small  $R$  values.

At large  $R$ , say  $R > 3.2$ , the heat transfer rate contributed by the region near the stagnation point ( $R < 3.2$ ) to the integral mean heat transfer rate on the surface was relatively small. Jet flow has the feature of bell-shape. The bell bottom increases with  $H$ , and  $Nu_{\max}$  generally occurs at the radial position corresponding to the size of this bottom. Therefore,  $H_{\max}$  corresponding to  $Nu_{\max}$  increased as  $R$  increased.

Equations (4) and (5) provide useful information for potential industrial applications concerned with determining the combinations of  $R$  and  $H$  values for

maximizing  $\overline{Nu}$  and the corresponding values  $\overline{Nu}_{\max}$  (Fig. 8).

### COMPARISON OF RESULTS

The predictions of the present correlation of  $\overline{Nu}$  [equation (2)] were compared with those obtained using the correlations of Schlunder [5] and of Goldstein *et al.* [10]. When  $H \geq 8$ , the predictions of the present correlation basically agreed with Goldstein's to within 10%, but deviated significantly at lower values of  $H$ . The term  $(24 - |H - 7.75|)$  in Goldstein's correlation implies that  $Nu_{\max}$  occurs at  $H = 7.75$  and is independent of the value of  $R$ , which is at variance with the present data (see Figs. 7-9). However, for  $H < 7.75$ ,  $Nu$  value from the correlation of Goldstein decreases linearly with  $|H - 7.75|$ .

The predictions of equation (2) were compared with those of Schlunder's [5] and Goldstein *et al.* [10] in Fig. 9. For  $H = 6$ ,  $R = 10$  and  $Re < 3 \times 10^4$ , the three correlations were in good agreement to within less than 15%. However, at higher  $Re$ , the correlations of Goldstein *et al.* and Schlunder were consistently lower than the present correlation; the difference between predictions decreased with  $Re$  reaching about 8% at  $Re = 6 \times 10^4$ . Results in Fig. 9 also showed that, as either  $H$  or  $R$  was decreased, the difference between the three correlations increased. In general, for  $H \leq 6$

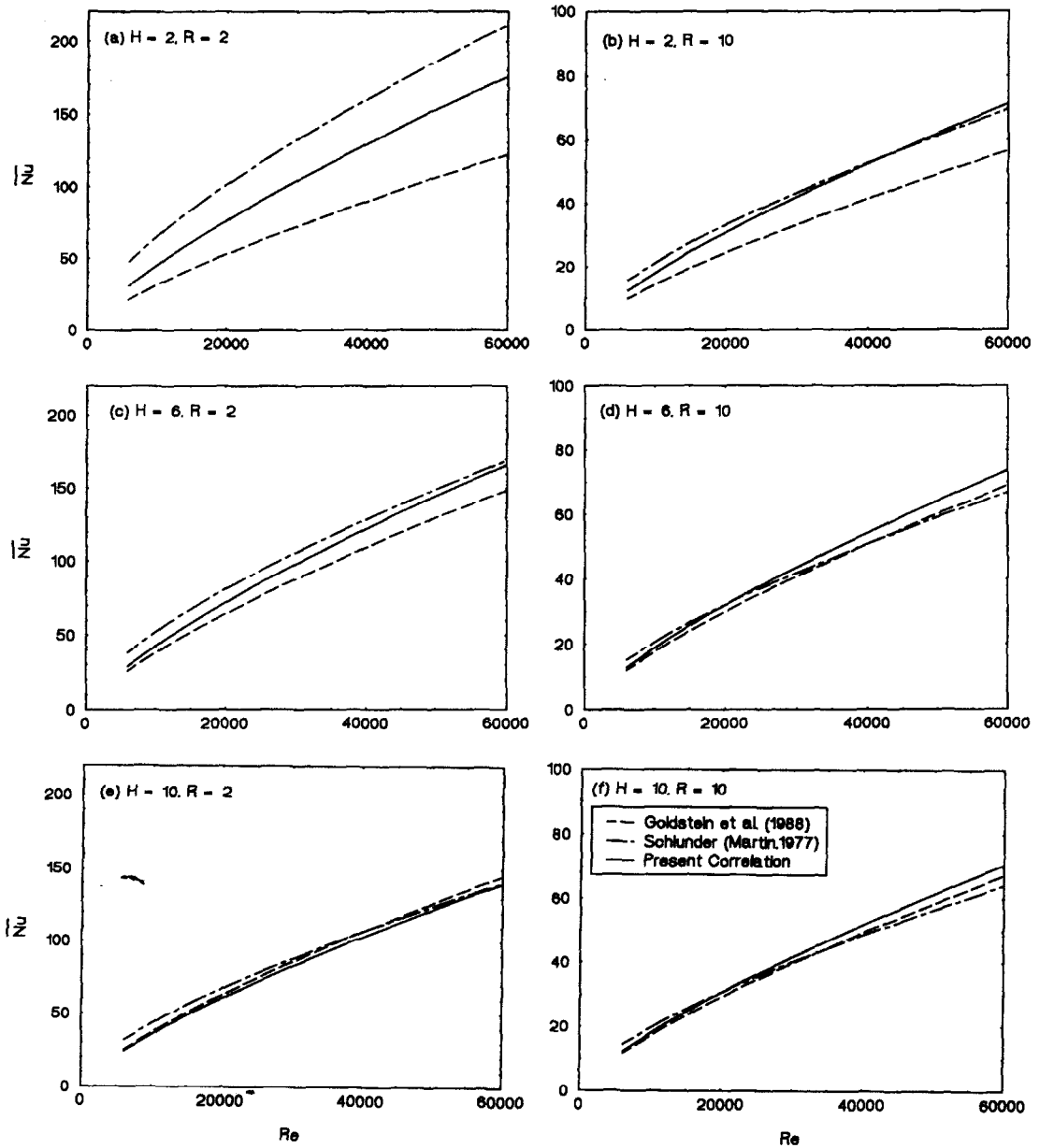


FIG. 9. Comparison of present correlation with those of Goldstein *et al.* [10] and Schlunder [5].

the predictions of Schlunder's and Goldstein's correlations were consistently higher and lower than those of the present correlation, respectively. However at higher  $H$ , the three correlations were in excellent agreement, Fig. 9.

As shown in Fig. 9a, when  $H = 2$  and  $R = 2$ ,  $\bar{Nu}$  predictions of Schlunder's correlation were higher than those of the present correlation by about 14% at  $Re = 6 \times 10^4$ , and by as much as 40% at  $Re$  of 6000. Conversely,  $Nu$  predictions of Goldstein's correlation were 32 and 50% lower than those of the present correlation at  $Re$  of  $6 \times 10^4$  and 6000, respectively. At  $H = 2$ , when  $R$  was increased from 2 to 10,  $Nu$  predictions by Schlunder's correlation were in good agreement with the present correlation, but those of

Goldstein's were still about 20% lower (see Fig. 9a and b).

**SUMMARY AND CONCLUSIONS**

Heat transfer experiments were performed to extend the present heat transfer data base to lower  $Re$  and jet spacing and to investigate the effects of  $R$  and  $H$  on both  $\bar{Nu}$  and  $Nu_{max}$ . The radial variation in the local and average Nusselt numbers was measured for a uniformly heated flat plate impinged by a circular air jet. In the experiments,  $Re$  varied from 6000 to 60 000,  $R$  from 0 to 10, and  $H$  from 1 to 12. Results showed that the maximum stagnation  $Nu$  occurred at  $H = 4.7$  and both  $\bar{Nu}$  and  $Nu_{max}$  were strong functions



of  $H$  and  $R$ . For  $H = 1$  and  $Re \geq 1.3 \times 10^4$ ,  $Nu_{\max}$  occurred at  $R = 1.8$ – $2$ , while at lower  $Re$  and/or higher  $H$ ,  $Nu_{\max}$  always occurred at the stagnation point ( $R = 0$ ). For  $H > 1$ , both  $\overline{Nu}$  and  $\overline{Nu}_{\max}$  increased with  $Re$ , but decreased with  $R$ . Results also showed that  $\overline{Nu}_{\max}$  was strongly dependent not only on  $H$  but also on  $R$ . While both  $\overline{Nu}$  and  $\overline{Nu}_{\max}$  increased with  $Re$ , the value of  $H$  corresponding to  $\overline{Nu}_{\max}$  was a strong function of  $R$ ; it decreased from  $\sim 4.7$  at  $R = 0$ , to as low as  $0.5$  at  $R = 3$ , then increased to  $\sim 5.7$  at  $R = 10$ . The values of  $\overline{Nu}$  and  $\overline{Nu}_{\max}$  were correlated in term of  $Re^{0.76}$ , equations (2) and (5), and the values of  $H_{\max}$  were correlated in terms of  $R$ , equation (4). Equations (4) and (5) provide useful information for potential industrial applications concerning about the combinations of  $R$  and  $H_{\max}$  values for maximizing the average Nusselt number as well as the corresponding values of  $\overline{Nu}_{\max}$ . Results suggested that the correlations of Goldstein *et al.* [10] and Schlunder [5] might be used to predict  $Nu$  at low  $Re$  and at  $H \geq 6$ , with a reasonable accuracy, but not at lower  $H$  values.

*Acknowledgments*—This research is sponsored by the University of New Mexico's Institute for Space Nuclear Power Studies (ISNPS). The authors are grateful to Dr Z. Guo of ISNPS for his help with the experimental setup and suggestions.

#### REFERENCES

1. K. P. Perry, Heat transfer by convection from a hot gas jet to a plane surface, *Proc. Inst. Mech. Engrs* **168**, 775–784 (1954).
2. R. Gardon and J. Carbonpue, Heat transfer between a flat plate and jets of air impinging on it, *International Heat Transfer Conference*, Part II, pp. 454–460 (1961).
3. R. Gardon and J. C. Akfirat, The role of turbulence in determining the heat-transfer characteristics of impinging jets, *International Heat Transfer Conference*, pp. 1261–1272 (1965).
4. K. Tataoka, T. Komai, and Nakamura, Enhancement mechanics of mass transfer in a turbulent impinging jet for high Schmidt number, *ASME Paper No.* 78-HT-5 (1978).
5. H. Martin, Heat and mass transfer between impinging gas jet and solid surfaces, *Advances in Heat Transfer* (Edited by T. Irvin and J. P. Hartnett), **13**, pp. 1–60. Academic Press, New York (1977).
6. R. N. Koopman and E. M. Sparrow, Local and average transfer coefficient due to an impinging row of jets, *Int. J. Heat Mass Transfer* **19**, 673–683 (1976).
7. R. J. Goldstein and A. I. Behbahani, Impingement of a circular jet with and without cross flow, *Int. J. Heat Mass Transfer* **25**, 1377–1382 (1982).
8. R. J. Goldstein and W. S. Seol, Heat transfer to a row of impinging circular air jets including the effect of entrainment, *Int. J. Heat Mass Transfer* **34**, 2133–2147 (1991).
9. L. G. Hansen and B. W. Webb, Air impingement heat transfer from modified surfaces, *Int. J. Heat Mass Transfer* **36**, 989–997 (1993).
10. R. J. Goldstein, A. I. Behbahani and K. K. Hellepplmann, Streamwise distribution of the recovery factor and the local heat transfer coefficient to an impinging circular air jet, *Int. J. Heat Mass Transfer* **29**, 1227–1235 (1986).
11. K. Jambunathan, E. Lai, M. A. Moss and B. L. Button, A review of heat transfer data for single circular jet imp, *Int. J. Heat Fluid Flow* **13**, 106–115 (1992).
12. W. M. Rohsenow, J. P. Hartnett and E. N. Ganic, *Handbook of Heat Transfer Application*. McGraw-Hill, New York (1985).
13. J. P. Holman, *Experimental Methods for Engineers*. McGraw-Hill, New York (1984).